Geothermics 106 (2022) 102573

Contents lists available at ScienceDirect

Geothermics

journal homepage: www.elsevier.com/locate/geothermics

Geochemical characterisation and modelling of the Luchon hydrothermal system (Central Pyrenees, France) and lessons learnt for the use of geochemical modelling techniques in granite-hosted alkaline thermal waters

Jon Jiménez *, María J. Gimeno, Luis F. Auqué

Earth Sciences Department, University of Zaragoza, C/Pedro Cerbuna, Zaragoza 50009, Spain

ARTICLE INFO

Keywords:
Geochemical modelling
Alkaline hydrothermal systems
Thermal waters
Geothermometry

ABSTRACT

Alkaline hydrothermal systems hosted in granitic rocks have been extensively investigated as natural analogues for radioactive waste disposal and for the geological storage of CO_2. Thereby, their geochemical characterisation provides useful information for the long-term performance assessment predictions. The geochemical modelling of one of these alkaline hydrothermal systems has been performed in Luchon (France), together with the application of different geothermometrical techniques to determine the temperature, pH and mineral equilibrium conditions at depth. The modelling results show that the main processes controlling the hydrogeochemical evolution of this system are: (1) the mixing between deep thermal and cold surface waters, (2) the conductive cooling and (3) the external input of CO_2. Other important results are that the most alkaline thermal waters are characterised by a high pH-buffering capacity during the mixing processes, and that the high pH values that characterise these thermal waters are not only inherited from the deep reservoir but strongly enhanced by conductive cooling. The reservoir temperature predicted by the geothermometrical modelling is in the range of 117 ± 8 °C, in good agreement with the temperatures ranging from 108 to 133 °C predicted by the classical geothermometers. The results of these calculations indicate as well that the thermal solutions have reached equilibrium with quartz, albite, potassium feldspar, zoisite and prehnite, and that a re-equilibirum with kaolinite and calcite is reached during their ascent to the surface. Another important outcome is that the precipitation of calcite in the deep reservoir could take place as a CO_2 mineral trapping mechanism in similar systems. Further, the sharp influence of the surface waters on the deep thermal waters reveals a high susceptibility of the system to potential contamination processes.

1. Introduction

The granite-hosted alkaline hydrothermal systems have been widely investigated in the context of geothermal exploration for a long time. However, in the last decades, the investigations of these systems have been extended to their study as natural analogues of the geological environments selected for the disposal of nuclear wastes, and this interest gave rise to several publications related to the geochemical study (composition, geothermometry, water-rock interaction, geochemical modelling, etc.) of the Pyrenean hydrothermal systems (e.g. Criaud and Vuataz, 1984; Iundt *et al.*, 1991; Alaux-Negrel *et al*; 1993 Auqué *et al.*, 1996a, 1996b, 1998; Asta *et al.*, 2010; 2012, 2017).

Additionally, granitic rocks have recently been investigated to assess their suitability for the geological storage of CO_2, through both, laboratory experiments (eg. Hangx and Spiers, 2009; Liu *et al.*, 2003; Ré *et al.*, 2014; Suto *et al.*, 2007) and experimental CO_2 injections in natural granite systems (e.g. Kaieda *et al.*, 2009 and Wakahama *et al.*, 2009). Since these experiments cannot deal with the time scale needed to reach the mineral equilibrium expected in the deep reservoirs in granitic systems (Ré *et al.*, 2014), their resuls have to be compared with those obtained from the characterization of the groundwaters and the modeling of the hydrogeochemical processes that take place in natural granite-hosted hydrothermal systems.

The Luchon system, located in the Pyrenean Axial Zone on the French slope of the Central Pyrenees, is included in the typology of alkaline hydrothermal systems hosted in granitic rocks, defined by

* Corresponding author.
E-mail address: jimenezbjon@unizar.es (J. Jiménez).

https://doi.org/10.1016/j.geothermics.2022.102573
Received 14 October 2021; Received in revised form 9 September 2022; Accepted 15 September 2022
Available online 29 September 2022

Michard and Roekens (1983). Several studies have been carried out on this system (e.g. Criaud and Vuataz, 1984; Iundt *et al.*, 1991; Alaux--Negrel *et al.*, 1993) but the use of geochemical modelling has been restricted to some geothermometrical calculations (Auqué *et al.*, 1996b, 1998) in the context of a regional study of different geothermal systems. The result is that the main processes that control the hydrogeochemical evolution of Luchon (mixing, conductive cooling and CO_2 transfer) have only been qualitatively reported in the previous investigations (e.g. Criaud and Vuataz, 1984).

These processes provide a suitable scenario for the study of the applicability conditions of geochemical modeling techniques used in similar granitic systems investigated for the geological storage of nuclear wastes and CO_2. Further, these processes may drastically change the evolution of certain parameters of interest in a geological storage. For instance, the mixing and CO_2 input control the pH buffering capacity of the groundwater, as well as the saturation indices of certain secondary minerals such as calcite, which could precipitate contributing to the CO_2 trapping. Further, some of these modelling techniques are used as well in granitic emplacements selected for the disposal of nuclear wastes that will be in contact with alkaline waters with geochemical characteristics and processes similar to the ones that characterise these hydrothermal systems. These are additional reasons for an accurate determination of

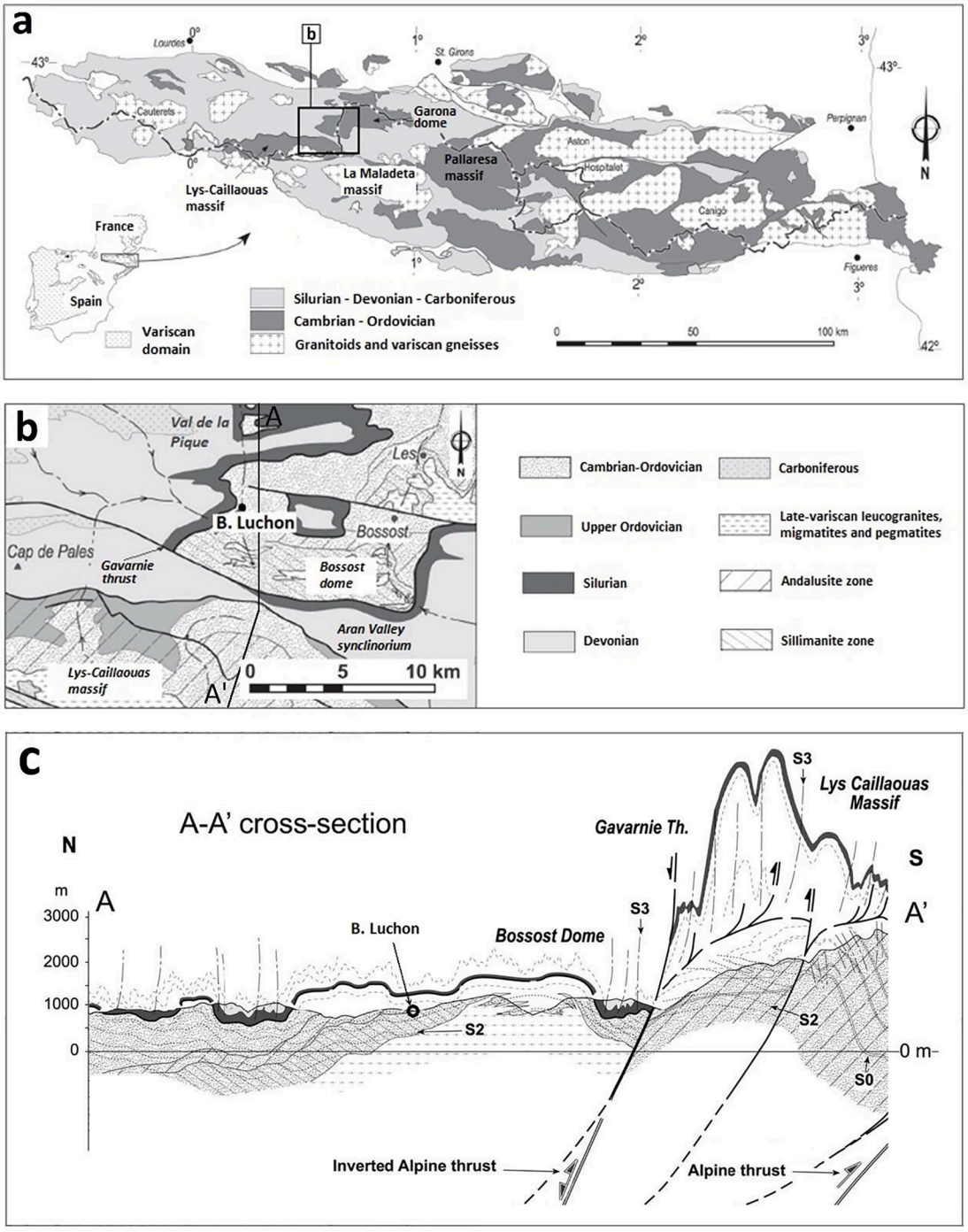

Fig. 1. Geological setting of the Luchon hydrothermal system: (a) Geological scheme of the Pyrenean Axial Zone; (b) Detailed geological scheme of the area studied indicated in panel (a), showing the main structures and materials, and indicating the location of Bagnères de Luchon; (c) Geological cross section of the study area, following the line A-A' indicated in panel (b). S0: bedding; S1, S2 and S3: foliation. Modified from Clariana et al. (2009).

the distinctive features and conditions of applicability that must be considered for the geochemical modelling of this type of waters.

On the basis of this background, the main objective of this study is to obtain a hydrogeochemical conceptual model of the Luchon system by quantifying the hydrogeochemical processes and determining the physical and geochemical conditions in the deep reservoir. The use of geochemical and geothermometrical modelling combined with the classical chemical geothermometers is needed to obtain this main aim. Additionally, considering the economic relevance of the Luchon system due to the use of its waters for balneotherapy and consumption, the study also aims to assess the possible practical implications of the hydrogeochemical model obtained, regarding the possible factors that could affect the water quality from a quantitative approach. The results of the modelling techniques applied here will also be compared with those obtained by similar techniques in other granitic alkaline systems, in order to assess the applicability conditions of these techniques in granite-hosted alkaline waters.

2. Geological setting

The hot springs of Bagnères de Luchon are located in the central part of the Pyrenean Axial Zone (Fig. 1.a), between the massifs of Lys (to the SO of Luchon) and Maladeta (to the SE), the Garonne dome (to the NNE) and the Aran valley synclinorium (to the E), within the western periclinal closure (Fig. 1.b) of the Bossots Dome (Bosch *et al.*, 1981), which is to the SSW of the Garona Dome. The outcroping rocks in the Luchon area are mainly Cambrian, Ordovician and Silurian. These materials were affected by a regional orogenic metamorphism during the Variscan Orogeny, reaching the cordierite-sillimanite zone (García-Sansegundo *et al.*, 2013). The metamorphic rocks are dominant in the area and are mainly represented by shales with biotite and shales with staurolite, andalusite and cordierite, and, to a lesser extent, quartzites, slates, banded mica-schists and marbles. Several outcrops of late Variscan plutonic igneous rocks are also present, associated to the Bossost Dome, which is constituted by leucogranites (granites, monzogranites and sienogranites) and pegmatitic sills (Vera, 2004). The sills are subvertical and subparallel to the main tectonic foliation (García-Sansegundo *et al.*, 2013). During their emplacement, these plutonic rocks crosscut the folds associated to the fourth stage of the Variscan deformation (Fig. 1.c) affecting the Cambrian, Ordovician, and Silurian rocks in the Bossost Dome area (Zwart and De Sitter, 1979).

The Luchon area is structurally characterised by a dominant array of Variscan fractures with W-E to WNW-ESE trends. The Alpine and Variscan thrusts with the same trends are also frequent, as well as a large-scale detachment level that gave rise to the elevation of the Bossots Dome during the alpine compression (García-Sansegundo *et al.*, 2013). The deformation is also represented by a family of N-vergent Variscan folds with W-E to NW-SE trends, that produced interference patterns with two other families of later Variscan lax folds, one W-E trending and the other one NNW-SSE trending (Clariana et al., 2009).

The Luchon hydrothermal system is hosted in the late Variscan granitic rocks of the Bossots Dome (Auqué *et al.*, 1998). The recharge area is not well defined, although it is mainly associated to the fractured granitic rock outcrops of the Bossost Dome that are located 6 to 8 km east of the thermal springs in Luchon (Chevalier-Lemire *et al.*, 1990) and are (due to a more intense fracturation) more permeable than the schists outcropping in most of the surface of the study area. Subsequently, the water infiltrated through the granite reaches depths over 5 km, acquiring temperatures of approximately 130°C (Chevalier-Lemire *et al.*, 1990), and residence times of about 14,000 years (Lopoukhine and Vigouroux, 1998). Finally, the thermal springs of this system result from the ascent of the thermal waters through the subvertical pegmatitic sills and their associated joints, as well as through some Variscan faults. These dikes or sills are embedded in the Cambrian-Ordovician sedimentary and metamorphic series (Bosch et al., 1981) and show dominant W-E and WNW-ESE trends, coinciding with the main Variscan fractures.

3. Methodology

Several datasets from the Luchon groundwaters (the analytical data are available in the annex of the online version, in Table A.I), obtained in several sampling campaigns by previous authors, have been selected for this study. The data belong to the studies of Alaux-Negrel *et al.* (1993), Criaud and Vuataz (1984) with data from 1983 and 1984, and Iundt *et al.* (1991). References to these publications will be abbreviated in several figures as follows, respectively: "Alaux-Negrel et al. (1993)"; "Criaud and Vuataz (1984)"; ""Iundt et al. (1991). Additionally, a new sampling campaign in 2019 was carried out for this study by the authors of this paper. Considering the large amount of analytical data, all samples have been renamed, both our own and the bibliographic ones, with a code from L1 to L32 (see Table I in supplementary material), in order to achieve a clearer graphical display. The analytical data correspond to the thermal springs and boreholes located in the Luchon spa resort, as well as to surface waters from the river La Pique and minor streams in the surroundings.

3.1. Sampling and chemical analysis

The methodology used in the previous sampling campaigns can be found in the original papers and, therefore, only the details of the sampling and analytical methods used for the last campaign in 2019 are described next. Two thermal springs from the Luchon spa and three cold surface waters were sampled. Temperature, pH and conductivity were measured *in situ*. From each spring, 2 bottles of polyethylene were taken, a 0.5 litter bottle for anion analysis and a 50 ml bottle for cation analysis. The water for cation analysis was filtered through 0.45 μm MILLIPORE filters and acidified with ultrapure HNO_3 to pH below 2. pH was measured using a pH-meter ORION 250 which also has a thermometer function. Conductivity was measured with a conductivity-meter Jenwey 470. The approximate errors in the measurement of pH, temperature and conductivity are ± 0.05 pH units, ± 0.5°C, and ± 0.3%, respectively.

Alkalinity was determined by a volumetric titration at pH = 4.5, by H_2SO_4 0.02 N. The analysis of F^- and Cl^- was carried out by the selective electrodes ORION 9409BN and ORION 9417BN, respectively. SO_4^{2-} was determined by turbidimetry in a molecular absorption spectrophotometer Thermo UV-10, in the Geochemistry Laboratory of the Earth Sciences Department of the University of Zaragoza. Ca, Mg, Na, K, Si and Li were analysed by ICP-AES (Inductively Coupled Plasma Atomic Emission Spectrometry), and Al by ICP-MS in the Analytical Services (SAI) of the same university. The charge balance error of the water analyses was calculated with PHREEQC and, in all cases, was less than 10% (and less than 5% in most of the samples), which is admissible according to Zhu *et al.* (2002).

3.2. Data processing and geochemical modelling

In the first step of the exploratory analysis, through the use of ion-ion diagrams, the linear correlation between the concentration of conservative elements has been used to identify and characterise water mixing processes. Sodium, whose behaviour is conservative in this system, has been selected as the tracer of the system evolution. This element has already been used as a tracer in previous studies of similar systems (e.g. Criaud and Vuataz, 1984; Asta *et al.*, 2010, 2017) and as in our case, it shows one of the highest correlation coefficients with the rest of the conservative elements (Si, F and Li). Other binary diagrams used here relate pH, Na and temperature, some of the most variable parameters in this system, which have been used to identify and characterise other hydrochemical processes such as differential conductive cooling and CO_2 transfer. Next, speciation − solubility calculations have been performed with the geochemical modelling software PHREEQC (Parkhurst

and Appelo, 2013) and the WATEQ4F thermodynamic database (Ball and Nordstrom, 2001). This database has been selected since it has been extensively contrasted for this type of calculations and it has provided consistent results in similar alkaline hydrothermal systems of the Pyrenees (e.g. Asta et al., 2010, 2012, 2017). The results of these calculations enable to determine the speciation of the dissolved components, the partial pressure of CO_2 and the saturation indices of the mineral phases of interest in the system. This code and database have also been used to perform the reaction path simulations, which include the identified mixing processes, conductive cooling and CO_2 transfer. The simulation results have been compared with the data of the natural system (analytical data) in order to test the validity of the final hydrogeochemical conceptual model.

3.3. Geothermometry

Chemical geothermometers consist of experimentally calibrated equations that represent heterogeneous chemical reactions dependent on temperature, that control the concentrations of certain elements in solution, so that they enable to determine the temperature of the water in the reservoir from the concentrations measured in the springs (Truesdell, 1976). These geothermometers are based on the assumption that the concentrations of the elements involved in the equations have not changed significantly due to water-rock interaction processes during the ascent of the hydrothermal solutions and that, therefore, the concentrations in the thermal springs are representative of the concentrations in the deep reservoir. This condition is frequently met in this type of granitic systems, since the rise of the water is fast enough to prevent mineral dissolution or precipitation (Auqué et al., 1996b). The geothermometers and calibrations selected for this study are indicated in Table 1. This selection is based on the mineralogy of the granitic rocks in which the hydrogeothermal system is hosted. On the basis of these criteria, the silica geothermometers SiO_2-quartz, SiO_2-chalcedony, K-F and the cationic geothermometers Na-K, Ca-K, Na-K-Ca, K-Mg, Li and Na-Li have been used. Also, several of these geothermometers have provided good results and have been considered as the most reliable in studies of similar geothermal systems (e.g. Auqué *et al.*, 1996b; Fournier and Truesdell, 1973; Porowski and Dowgiałło, 2009).

Finally, to complement these calculations and check the possible effects of secondary processes, several geothermometrical modelling simulations have also been performed. These calculations consist of simulating the progressive increase in temperature of a water sample collected from a thermal spring, and calculating the evolution of the saturation indices of a group of selected phases with the temperature increase. The temperature range in which most of the saturation indices converge to equilibrium, can be assumed as representative of the water temperature in the deep reservoir (Reed and Spycher, 1984; Bethke, 1996). Several simulations have been carried out with PHREEQC, assuming that equilibrium is reached in the reservoir with the phases likely to be present in the hosting lithology.

The selected mineralogy includes the most common phases in granitic rocks, such as quartz, chalcedony, albite, K-feldspar and some phases likely to be present in these systems as secondary minerals such as calcite and kaolinite, as suggested by Choi *et al.* (2014). These secondary phases, along with other aluminosilicates are the most common alteration and fracture filling minerals in granitic rocks (White *et al.*, 2005, 1999; and references therein). Calcite is frequently included in the equilibrium association in similar granite-hosted systems with alkaline waters for the geothermometrical simulations (e.g. Michard and Roekens, 1983; Auqué *et al.*, 1998; Asta *et al.*, 2012) and the same is applicable to prehnite, zoisite, and laumontite (e.g. Michard and Fouillac, 1980; Michard and Roekens, 1983; Auqué et al., 1996b, Auqué *et al.*, 1998), which have been added as auxiliary phases in the simulations. As for the previous geochemical modelling (speciation-solubility and reaction path calculations) the WATEQ4F thermodynamic database has been used for the geothermometrical calculations. However, a sensitivity analysis has been performed with the PHREEQC.dat database, modified by Appelo et al. (2014) to be used for temperatures from 0 to 200 °C. The results obtained with both databases are very similar and, therefore, only the results obtained with the PHREEQC.dat database are shown here. Additionally, thermodynamic data for albite, potassium feldespar, chalcedony, prehnite, zoisite, kaolinite and laumontite have been taken from Michard (1983), because they have been frequently used with good results in similar granitic systems (e.g. Asta et al., 2012, and references therein).

Table 1
Chemical geothermometers and calibrations used in this study. Concentration units for the elements involved are all in mg/L. In the Na-K-Ca geothermometer with the calibration from Fournier and Truesdell (1973), β = 4/3 should be used if the temperature obtained is lower than 100 °C; if with that value of β the temperature is higher than 100 °C, the temperature should be recalculated considering β = 1/3.

Geothermometer	Calibration	Author
SiO_2-quartz	$T = \frac{1315}{5.205 - log(SiO_2)} - 273.15$	Truesdell (1976)
	$T = \frac{1309}{5.19 - log(SiO_2)} - 273.15$	Fournier (1977); Fournier and Potter (1982)
SiO_2-chalcedony	$T = \frac{1032}{4.69 - log(SiO_2)} - 273.15$	Fournier (1977); Fournier and Potter (1982)
	$T = \frac{1112}{4.91 - log(SiO_2)} - 273.15$	Arnòrsson et al. (1983)
Na-K	$T = \frac{855.6}{0.857 + \log(Na/K)} - 273.15$	Truesdell (1976)
	$T = \frac{1170}{1.42 + \log(Na/K)} - 273.15$	Michard (1990)
Ca-K	$T = \frac{3030}{3.94 + \log(Ca/K)} - 273.15$	Michard (1990)
Na-K-Ca	$T = \frac{1647}{\log(Na/K) + \beta[\log(\sqrt{Ca}/Na) + 2.06] + 2.47} - 273.15$	Fournier and Truesdell (1973)
Li	$T = \frac{2258}{1.44 + \log(Li)} - 273.15$	Fouillac and Michard (1981)
Na-Li	$T = \frac{1040}{0.43 + \log(Na/Li)} - 273.15$	Michard (1990)
	$T = \frac{1000}{0.38 + \log(Na/Li)} - 273.15$	Fouillac and Michard (1981)
K-Mg	$T = \frac{4410}{13.95 - \log(K^2/Mg)} - 273.15$	Giggenbach et al. (1983)
K-F	$T = \frac{2170}{1.79 - \log(K \cdot F)} - 273.15$	Michard (1990)

4. Results and discusion

4.1. General hydrogeochemical characteristics and processes in the system

The waters of the Luchon system are characterised by spring temperatures between 10 and 74°C, low mineralisation, pH values between 6.97 and 9.48, sodium concentrations between 0.065 and 4.37 mmol/L, and Mg concentrations between $5.5 \bullet 10^{-4}$ and 0.305 mmol/L. The thermal samples with the highest temperatures are characterised by high pH values, the presence of Na as the dominant cation and the absence of a dominant anion, a sulphurous character and very low Mg concentrations. These general geochemical characteristics of the thermal waters enable to include them in the typology called "alkaline thermal waters hosted in granitic rocks" (Michard and Roekens, 1983). Other important features of the thermal waters in this system are the low CO_2 partial pressures and the S.I. of calcite close to equilibrium (see Table II in the supplementary material). However, one of the most

outstanding characteristics of the system is that despite their proximity, that suggests a common deep reservoir, the springs show a wide variability in salinity, pH and temperature. To analyse the evolution of these parameters, the diagrams silica vs. sodium (Fig. 2.a), sodium vs. temperature (Fig. 2.b and 2.c) and pH vs. sodium (Fig. 2.d) have been plotted.

Fig. 2.a shows a strong linear correlation between the concentrations of the most conservative elements in the system (Na and Si). It is also important to indicate that the highest concentrations correspond to the fluids of the hottest springs and the lower concentrations correspond to the colder ones (see Figure 2.b). This behavior, together with the high linear correlation observed, indicates the existence of mixing between deep thermal waters (thermal end members, L1, L22 and L20; Fig. 2.c) and surface cold waters (cold end member L13) in the Luchon hydrothermal system. The linear correlation involving samples from the same springs but from different years indicates that the mixing process, the temperatures and the mixing ratios are fundamentally stable over time, at least in the short term. The theoretical mixing path is also shown in Fig. 2.c, where the temperature evolution is expressed as cooling (considering the temperature of 74°C, measured in the hottest sample, L20, as the reference temperature). Two trends can be observed: a decreasing linear trend corresponding to the cooling by mixing, and several trends of additional cooling that move the positions of the samples towards the right of the mixing line. This additional cooling can be interpreted as conductive cooling, associated with longer ascent paths or lower flows of the waters in certain springs. There is a third trend, represented by samples L5 and L21 only (both from the spring Ferruginese sampled in 1984, L5, and 1991, L21), which shows a less extensive cooling than would be expected by mixing, that is, the samples plot to the left of the mixing line. This result confirms what was qualitatively indicated by Criaud and Vuataz (1984), that this spring has undergone conductive heating by thermal equilibrium with the hot rocks. The heating can be quantified from Fig. 2.c as about 13°C.

Another important parameter with a high variability in the system is pH, and Fig. 2.d displays its evolution during the mixing represented by the Na concentration. The pH values decrease as the sodium concentration and temperature decrease, that is, as the proportion of the cold end-member increases during mixing. The higher pH values are associated to the higher sodium concentrations (approximately in the range of 3.5 – 4.5 mmol/L in the thermal alkaline waters) and these high values are maintained down to sodium concentrations close to 1.5 mmol/L, near the cold end member. This slow decrease indicates a high pH buffering capacity in the alkaline thermal solutions, which is related to the presence of high concentrations of some active acid-base pairs ($H_4SiO_4^0/H_3SiO_4^-$ and HCO_3^-/CO_3^{2-}) in these waters (the speciation-solubility calculations are available in the supplementary material in Table II).

Most of the samples fit to a logarithmic trend in Fig. 2.d and, since these samples represent mixing (as seen in Fig. 2.b and 2.c), it is likely that this logarithmic trend of the pH values represents the mixing path. Nevertheless, this can only be confirmed by the theoretical simulation of the mixing process and the evaluation of the pH evolution (see section 4.3). Another interesting result is that the thermal end members L1 and L22 have different pH values, despite the fact that their temperature and concentration of sodium are almost the same (see Fig. 2.c). This difference suggests the effect of a secondary process likely to be related to CO_2 transfer, since this process would modify pH without affecting the temperature or the sodium concentration.

Fig. 3 shows the CO_2 partial pressure obtained with the PHREEQC calculations in all the samples. There is an inverse correlation between the CO_2 partial pressure and the pH and a wide range of CO_2 partial pressures (log pCO_2 = -4.59 to log pCO_2 = -2.59) with most of the samples clearly in disequilibrium with the atmospheric value of log pCO_2 = -3.5. Samples with CO_2 partial pressures above the atmospheric partial pressure are susceptible to lose CO_2 under surface conditions, while those with values below the atmospheric partial pressure are susceptible to gain CO_2. Thereby, in the case of L22 and L1, the different pH value can be justified by the different CO_2 partial pressure shown in Fig. 3 (log pCO_2 = -3.51 and - 3.38 respectively) that would be consistent with a CO_2 gain from L22 to L1. This CO_2 contamination can differentially affect the waters of different springs, and may be related to edaphic or biological processes (e.g. Asta *et al.*, 2010, 2017).

4.2. Geothermometry

4.2.1. Chemical geothermometers

The results obtained by applying the selected chemical geothermometers and calibrations (Table 1) to the selected thermal waters are shown in Table 2. Regarding the silica geothermometers all calibrations have provided similar temperatures although those obtained with SiO_2 - chalcedony are lower (89 – 102°C) than the ones provided by SiO_2 – quartz (117 to 129°C). With respect to the cationic geothermometers (Na-K, K-Mg, Ca – K, Na – K – Ca, Li and Na-Li) the temperatures calculated range from 100 to 141 °C, in a better agreement with the temperatures predicted by SiO_2 – quartz compared to those predicted by SiO_2 – chalcedony.

In the case of the Na-K-Ca geothermometer, using the Fournier and Truesdell (1973) calibration, only the results obtained with β=4/3 (109 – 115°C) have been considered valid since they are consistent with the temperatures obtained with the other geothermometers and the geothermometrical simulation (see next section). Other authors (e.g. Vandelannoote, 1984; Michard *et al.*, 1986, 1989; Auqué *et al.*, 1996b) have also verified that this geothermometer provides results consistent with the rest of the geothermometrical techniques considering a value of β=4/3 in its calibration, even when the temperature at depth exceeds 100°C (a situation in which Fournier and Truesdell, 1973, recommend the use of β=1/3).

It is also interesting that the Na-Li geothermometer provides slightly lower temperatures than the rest of the cationic geothermometers (Table 2), although the Na-Li geothermometer with the calibration of Fouillac and Michard (1981) provides a temperature estimation of 127°C for sample L1, similar to the temperature estimated by SiO_2 – quartz and slightly higher than those given by the Na-K or Na-K-Ca geothermometers. On the other side, the Na-Li calibration of Michard (1990) provides exceedingly high temperatures (135 and 141 °C) compared to most of the other geothermometers. Thus, only the Na-Li calibration of Fouillac and Michard (1981) has been considered reliable for this system, so that the temperatures obtained with the calibration of Michard (1990) will not be considered for the temperature ranges provided in the next sections. Regarding the K-F geothermometer, although obtained by a poor but significant correlation between K and F for several thermal alkaline waters in granites (Michard, 1990), it provides temperatures between 114 and 121 °C in this system, in good agreement with the temperatures provided by most of the other geothermometers used.

Finally, another important result that will be discussed later is the fact that the cationic geothermometers applied to sample L20 provide significantly lower temperatures than the same geothermometers applied to samples L1 and L22.

4.2.2. Geothermometrical modelling

The selected mineral phases used for the geothermometrical simulations are those expected to participate in the control of the composition of the Luchon thermal waters and are the same considered in other similar systems (Michard and Fouillac, 1980; Michard and Roekens, 1983; Michard et al., 1986, 1989; Auqué et al., 1998; Buil et al., 2006; Asta et al., 2012): albite, K-feldspar, quartz (or chalcedony), calcite, kaolinite and some calcium aluminosilicates as auxiliary phases (laumontite, prehnite and zoisite). All these phases have been included in the calculations performed using samples L1 and L22 (L20 does not have available Al concentration data). The simulations have been carried out considering closed and open system conditions (without and with mass

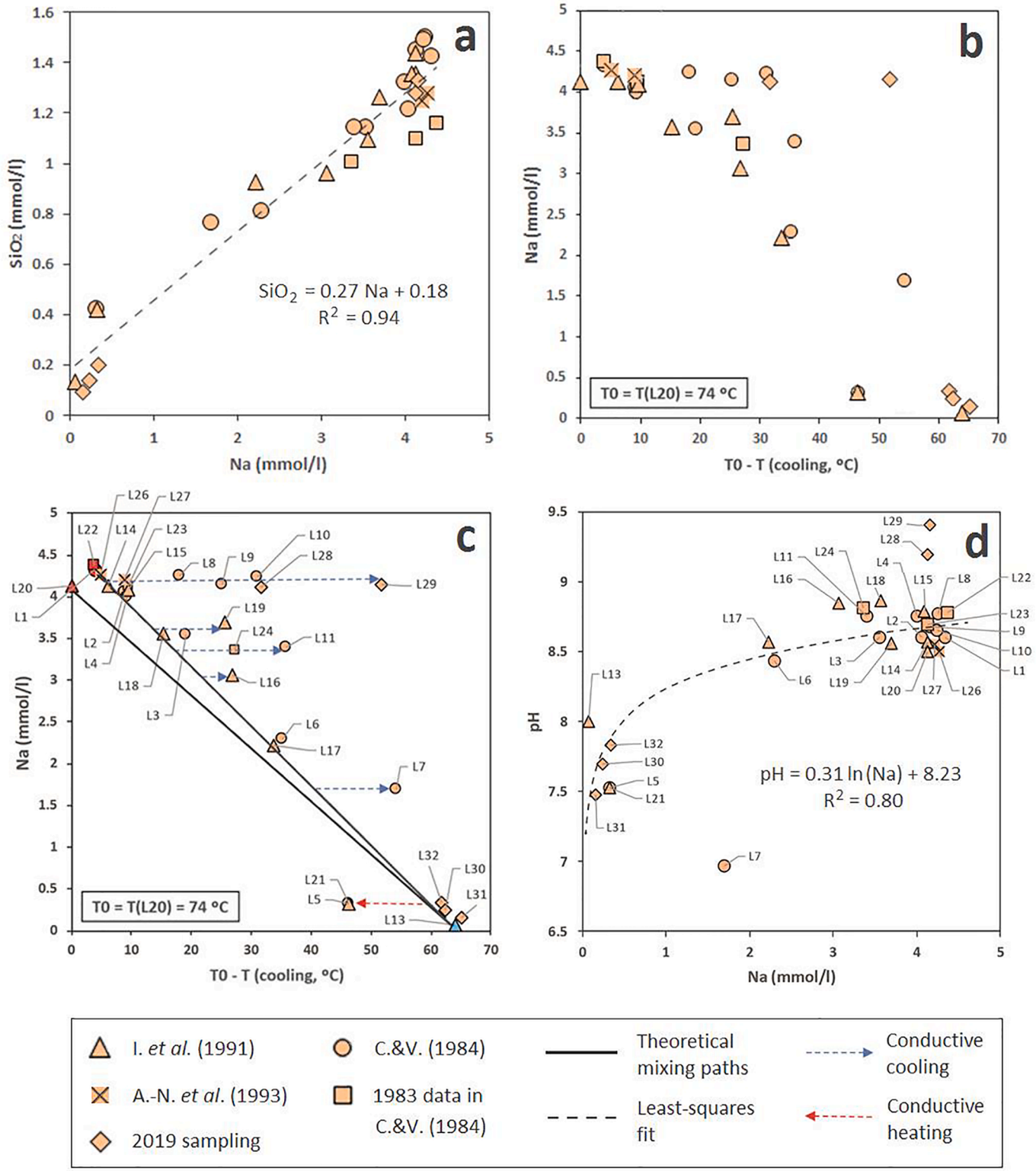

Fig. 2. Diagrams displaying the relation between sodium and silica concentrations (a), sodium and temperature (b and c) and sodium and pH (d) in all the samples of the Luchon thermal springs and surface waters. (a) Ion-ion diagram showing the correlation between the concentrations of the most conservative elements in the system and the fit obtained by linear least squares; (b) Na concentration vs. temperature diagram, where temperature is represented as cooling with respect to the maximum temperature of the samples (74 °C); (c) Shows the same data as (b) but the theoretical mixing (dashed lines) and conductive cooling and heating (dotted arrows) paths have been plotted. The theoretical mixing paths show that mixing takes place between the most representative waters of a thermal end member (L1, L20 and L22) and a cold end member (L13). The cooling and heating paths show the extra cooling or heating, respectively, that a sample has suffered over the one expected only by mixing (see explanation in the text). The thermal and cold end members are shown in red and blue, respectively, as will be in the following figures. (d) Shows the sodium concentration with respect to pH and the logarithmic fit of all the samples, without considering samples L7, L28 and L29 (see explanation in the text).

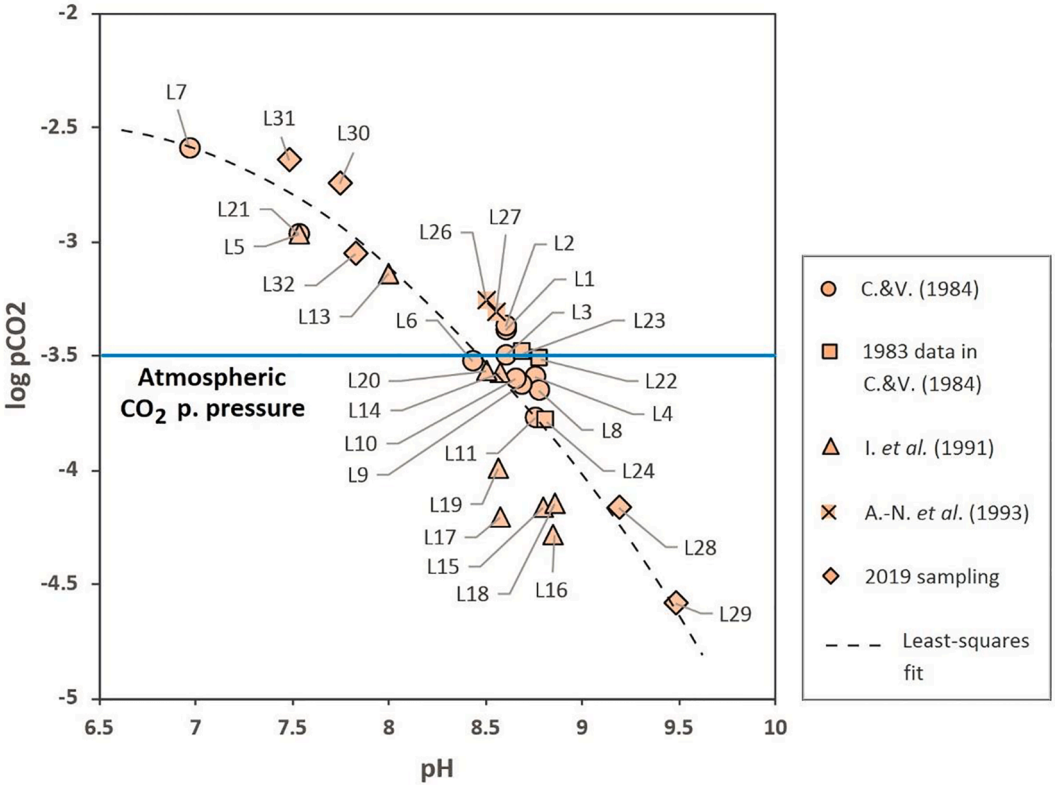

Fig. 3. CO_2 partial pressure vs. pH diagram. The least-squares fit to all the samples has been represented, as well as the atmospheric CO_2 partial pressure (horizontal line at log pCO_2 = - 3.5). The CO_2 partial pressure of each sample has been calculated in atm with PHREEQC and the thermodynamic database WATEQ4F.

Table 2
Temperatures (°C) obtained with the geothermometers and calibrations used for the thermal end-member samples (L1, L20 and L22) considered in this study. There was no Li data available for sample L20.

Geothermometer	Calibration	T (°C)		
		L1	L20	L22
SiO_2-quartz	Truesdell (1976)	128	129	118
	Fournier (1977); Fournier and Potter (1982)	128	129	117
SiO_2-chalcedony	Fournier (1977); Fournier and Potter (1982)	101	102	89
	Arnòrsson et al. (1983)	100	101	89
Na-K	Truesdell (1976)	117	100	111
	Michard (1990)	119	106	114
Ca-K	Michard (1990)	118	111	118
Na-K-Ca (β = 4/3)	Fournier and Truesdell (1973)	114	109	115
Na-K-Ca (β = 1/3)	Fournier and Truesdell (1973)	147	138	145
Li	Fouillac and Michard (1981)	108	–	111
Na-Li	Fouillac and Michard (1981)	127	–	133
	Michard (1990)	135	–	141
K-Mg	Giggenbach et al. (1983)	120	–	118
K-F	Michard (1990)	121	114	121

transfers, respectively), in the latter case imposing a reequilibrium with kaolinite and calcite. The re-equilibrium with kaolinite has been simulated following the recommendations and observations from previous authors (e.g. Michard and Roekens, 1983; Michard et al., 1986; Auqué et al., 1998; Asta et al. 2012). In the case of calcite, the reequilibrium has been considered regarding the PHREEQC speciation-solubility results (see Table A.II in the supplementary material) which show that the thermal end-members (L1, L20 and L22) are very close to equilibrium with calcite, as reported earlier in many alkaline thermal waters under different spring temperatures (e.g. Asta *et al.*, 2012, and references therein). The simulations have been performed in 100 steps, through which temperature has been increased from the value measured in the spring up to 150°C.

Simulation results are displayed in Fig. 4, which shows that the evolution of the saturation indices only gets an admissible convergent point when besides the increase in temperature, the simulation imposes re-equilibrium with kaolinite and calcite. The effect of re-equilibrating with kaolinite can be seen comparing Fig. 4.a - 4.b and 4.c - 4.d, since without imposing this re-equilibrium, no convergence of the saturation indices is obtained. The effect of re-equilibrating with calcite can be observed comparing Fig. 4.c - 4.d and 4.e - 4.f, with a higher convergence of zoisite and prehnite with respect to the mean equilibrium temperature.

As already reported in previous studies in other granitic systems (e.g. Auqué *et al.*, 1998) the two deduced re-equilibrium processes do not significantly affect the pH of the hydrothermal solutions during the ascent. In agreement with this, the simulations indicate low rates of calcite dissolution from 0.057 to 0.059 mmol/L and of kaolinite precipitation from 0.07 to 0.1 mmol/L. However, as shown in Fig. 4, these small mass transfers are enough to give a more precise result for the geothermometrical simulations. This is consistent with the fact that the S.I. of several of the phases considered depend on the Ca (in the case of zoisite and prehnite) and Al (in the case of zoisite, prehnite, KF and albite) concentrations, controlled in turn by the re-equilibrium with calcite and kaolinite, respectively. Comparing all the simulation results obtained under different mass transfer conditions, the set of phases that reach equilibrium at almost the same temperature (Fig. 4.e and 4.f) are albite, quartz, potassium feldespar, calcite, kaolinite, zoisite and prehnite, which in the case of L1 converge at a temperature of 118 ± 7°C, whilst they do it at 113 ± 4°C for sample L22. The pH values calculated for the deep reservoir range from 8.1 to 8.3, which are significantly lower than those observed in some springs (up to 9.48). This result will be recalled later, in the simulation of the secondary processes.

Finally, regarding the agreement between geothermometers and simulation results, the fact that the cationic geothermometers Na-K, K-

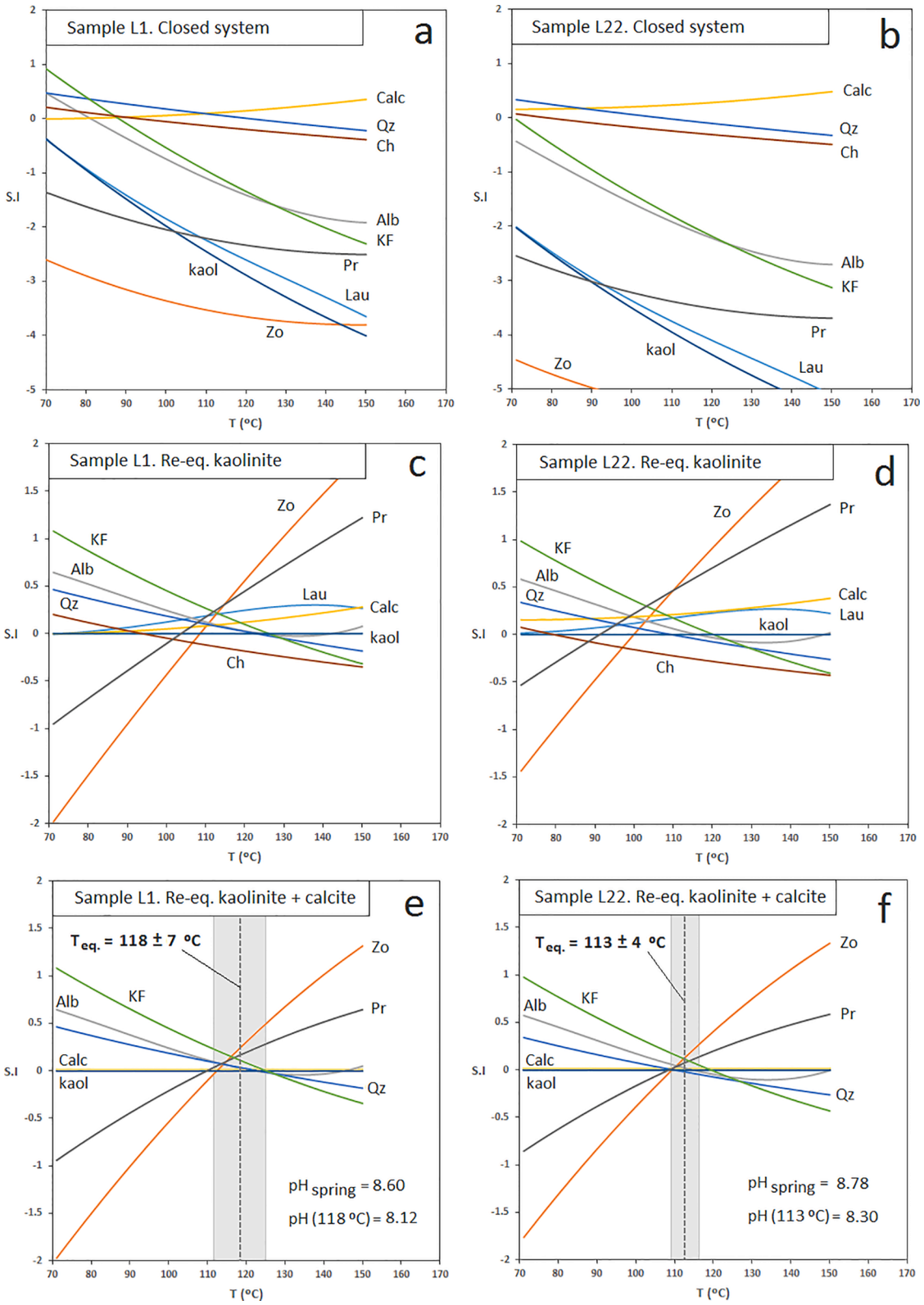

Fig. 4. Results of the geothermometrical simulations performed with PHREEQC and applied to the thermal end member samples L1 and L22. The text included in the figures indicates the simulation conditions, the mean equilibrium temperature and the uncertainty range (expressed as the standard deviation, shaded band), as well as the pH measured at the spring and the pH calculated in the simulation for equilibrium conditions (the pH value in the deep reservoir). (a) and (b): simulation under closed system conditions. (c) and (d): simulation imposing are-equilibrium with kaolinite. (e) and (f): simulation imposing a constant re-equilibrium with kaolinite and calcite, but plotting only the S.I. of the phases with which the thermal solutions are most likely to be in equilibrium, according to the rest of simulation results. Abbreviations: Alb (albite), Calc (calcite), Kaol (kaolinite), KF (potassium feldespar), Qz (quartz), Ch (Chalcedony), Lau (laumontite), Pr (prehnite), Zo (zoisite).

Mg, Ca-K, Na-K-Ca, Li and Na-Li, provide temperature values in the range 100 – 133°C similar to the range obtained from the geothermometrical simulations, 117 ± 8°C, is noteworthy. The temperatures provided by the Si-quartz geothermometer are also in a similar range, from 117 to 129°C but the values obtained by the Si-chalcedony geothermometer are lower. This difference between the Si-quartz and Si-chalcedony results is consistent with the fact that the solution cannot be simultaneously in equilibrium with both phases and in this case quartz seems to be the phase with which the groundwater is in equilibrium at depth.

4.3. Modelling of the secondary processes

4.3.1. Theoretical simulations

The occurrence of mixing with superimposed conductive cooling and CO_2 contamination at surface has been deduced and characterised based on the exploratory analysis explained above (section 4.1 and Fig. 2). However, in order to validate these results with a quantitative approach, these processes have been simulated with PHREEQC and the WATEQ4F thermodynamic database.

The simulation results have been plotted in the pH vs. temperature diagram shown in Fig. 5. The simulation of mixing has been implemented by considering L22 and L13 as the thermal and cold end members, respectively, as previously deduced from the Na vs. cooling diagram (Fig. 2.c). It has been developed in 10 steps that represent the mixing of different proportions of the two end members, that is, from 100% of L22 and 0% of L13, to 0% of L22 and 100% of L13. The resulting pH and cooling values in each step have been plotted with a green diamonds mixing path. The conductive cooling of the thermal end member L22 has also been simulated. It has been performed in 12 steps, by cooling the L22 from 70.1°C to 10°C. The pH and cooling values obtained in each step have been plotted with a yellow squares cooling path. Additional cooling simulations have been carried out using the result for different mixing proportions between L22 and L13, as initial solutions.

The final simulation has been the CO_2 input, which has been implemented by dissolving variable amounts of this gas into the thermal water L22. This simulation has been carried out in 10 steps and the reaction path has been indicated with a vertical pCO_2 scale showing the isothermal pH decrease due to CO_2 contamination. Finally, the mixing between the theoretically obtained CO_2-contaminated solutions and the cold end member L13 has also been simulated, using the same procedure as indicated for the previous mixing simulations, and the mixing paths have been plotted with dotted lines, but not showing the discrete theoretical solutions, in order to obtain a clearer graphical display.

The results shown in Fig. 5 can be summarised as follows:

- The mixing simulations between the thermal and the cold end members show a non linear decrease of pH as the cold end member proportion increases. There is a clear pH buffering effect on the alkaline thermal waters that remains effective up to mixing proportions of the two end members close to 50%.
- The conductive cooling simulations show a linear increase in pH, with a variation rate of 0.0135 pH units per degree°C of cooling. These simulations have been performed over initial solutions with different mixing ratios between L22 and L13 and the pH variation rate remains almost constant regardless of the mixing proportions. This is consistent with a similar pH control by the equilibrium

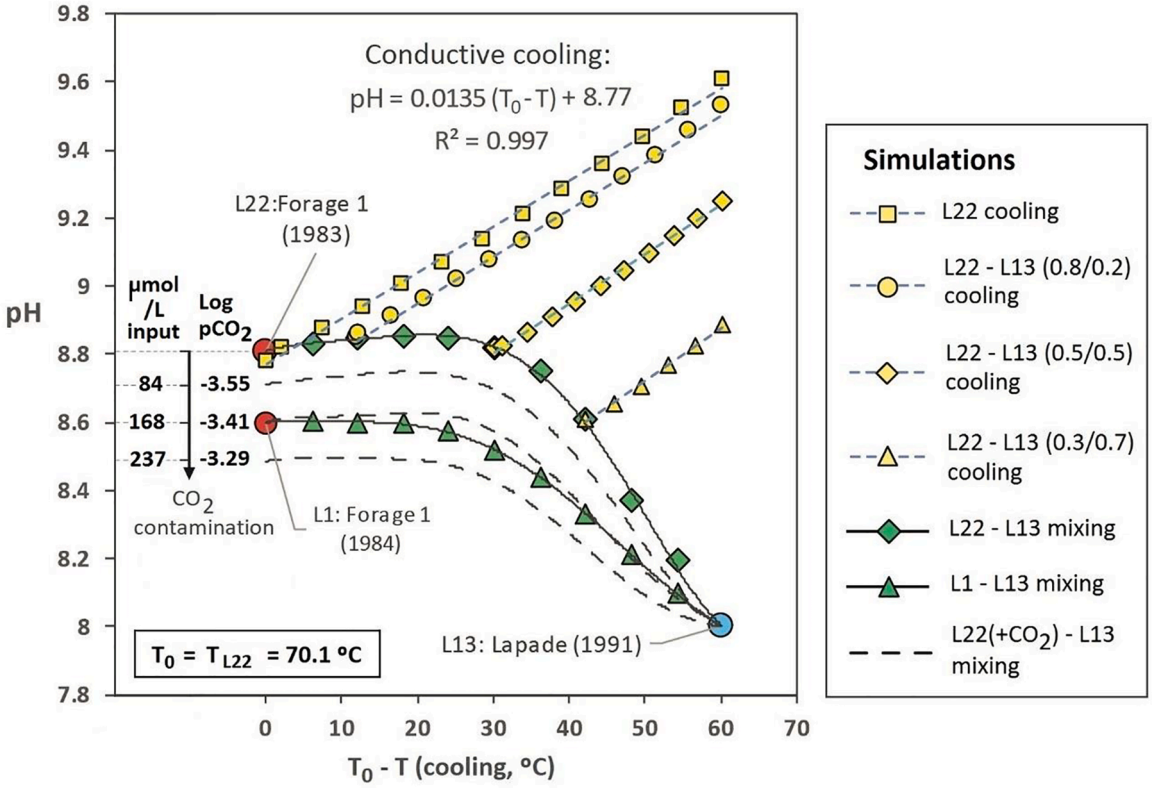

Fig. 5. Simulation results for the secondary processes, performed with PHREEQC and represented in the pH vs. cooling plot (see explanation in the text). The mixing simulations include: the mixing between the thermal end members L1 and L22 and the cold end member L13, as well as between theoretical solutions and the cold end member L13. These theoretical solutions were obtained by simulating the CO_2 contamination with different added amounts of this gas until the value of log $pCO_2 = -3.41$ predicted by the speciation-solubility calculations for L1 has been obtained (input of 168 µmol/L CO_2). The results of the cooling simulations are shown for different mixing ratios between L22 and L13. The function obtained for these simulations by linear least squares, that remains almost constant regardless of the mixing ratios, is also indicated.

constants of the acid-base pairs in solution, that increase linearly with cooling.

- The CO_2 contamination simulations, specifically the addition of 168 μmol/L of CO_2, has enabled to reproduce the L1 characteristics of pH and pCO_2, supporting thereby the previous hypothesis of CO_2 contamination at the surface (see section 4.1). The mixing process between the resulting solution and the cold end member L13 has also been simulated and the mixing path obtained is very similar to the mixing path between L22 and L13. This result indicates the feasibility of an evolution process characterised by mixing between a thermal end member that has first undergone CO_2 contamination (L1), and the cold end member L13.

4.3.2. *Comparison between the simulation of the secondary processes and the analytical data for the natural system*

The set of simulations presented in the previous section indicates that the hydrogeochemical evolution of the thermal solutions in Luchon during their ascent is characterised by mixing, conductive cooling and contamination with CO_2 at the surface. The theoretical simulations of these processes are validated in this section by displaying together the simulation results and the values from the real samples (Fig. 6). Additional simulations to those in the previous section have been carried out here as an uncertainty assessment to the selected end members in order to consider the entire range of variability of the samples. These simulations include the mixing between the three possible thermal end members (L22, L1 and L20) and the L13 cold end member, the mixing with a "pH-restored L13 end-member", and the conductive cooling of different thermal end members.

Fig. 6 shows that most of the samples fit in the models by different combinations of mixture, conductive cooling and/or CO_2 transfer. However, a better fit is obtained if a theoretical solution resulting from neutralising the anomalous pH of L13 (pH = 8) is considered as a cold end member (Figure 6.b). That anomalous pH (see Fig. 2.d) is restored to the value corresponding to the logarithmic trend obtained for the pH evolution by mixing. The adjustment has been calculated with the analytical sodium concentration in L13, using this value in the expression (Eq. (1)) of the logarithmic trend line (see Fig. 2.d):

$$pH = 0.3117 \cdot \ln(Na) + 8.23 \quad (1)$$

where Na is expressed in mmol/L. A theoretically adjusted or "neutralised" pH value of 7.38 is obtained for L13. This pH is more representative of the surface water sampled in La Pique river (L31), which collects the water from the shallow alluvial aquifer, that is, the cold end-member in the mixing process. The theoretically neutralised solution provides a better fit between the simulations and the analytical data (Fig. 6b), and the original anomalous pH is probably related to the variable CO_2 exchange at surface.

Whith the mixing lines between L1 / L22 and the neutralised L13, most of the samples interpreted as affected by conductive cooling from the binary plots (Fig. 2.c) fit on the theoretical single conductive cooling paths that plot above the theoretical mixing line. The rest of the samples, not affected by conductive cooling, fit reasonably well on the theoretical pure mixing paths. Finally, the conductive heating result affecting samples L5 and L21 in Fig. 6.b shows approximately 10°C, which is consistent with the 13°C deduced from Fig. 2.c.

In summary, the results shown in Fig. 6 confirm the initial hypothesis of mixing between thermal waters and a cold surface water reservoir with the superimposed effects of differential CO_2 contamination and conductive cooling affecting some springs. The CO_2 input simulations have also confirmed that the thermal end member L1 can be the result of

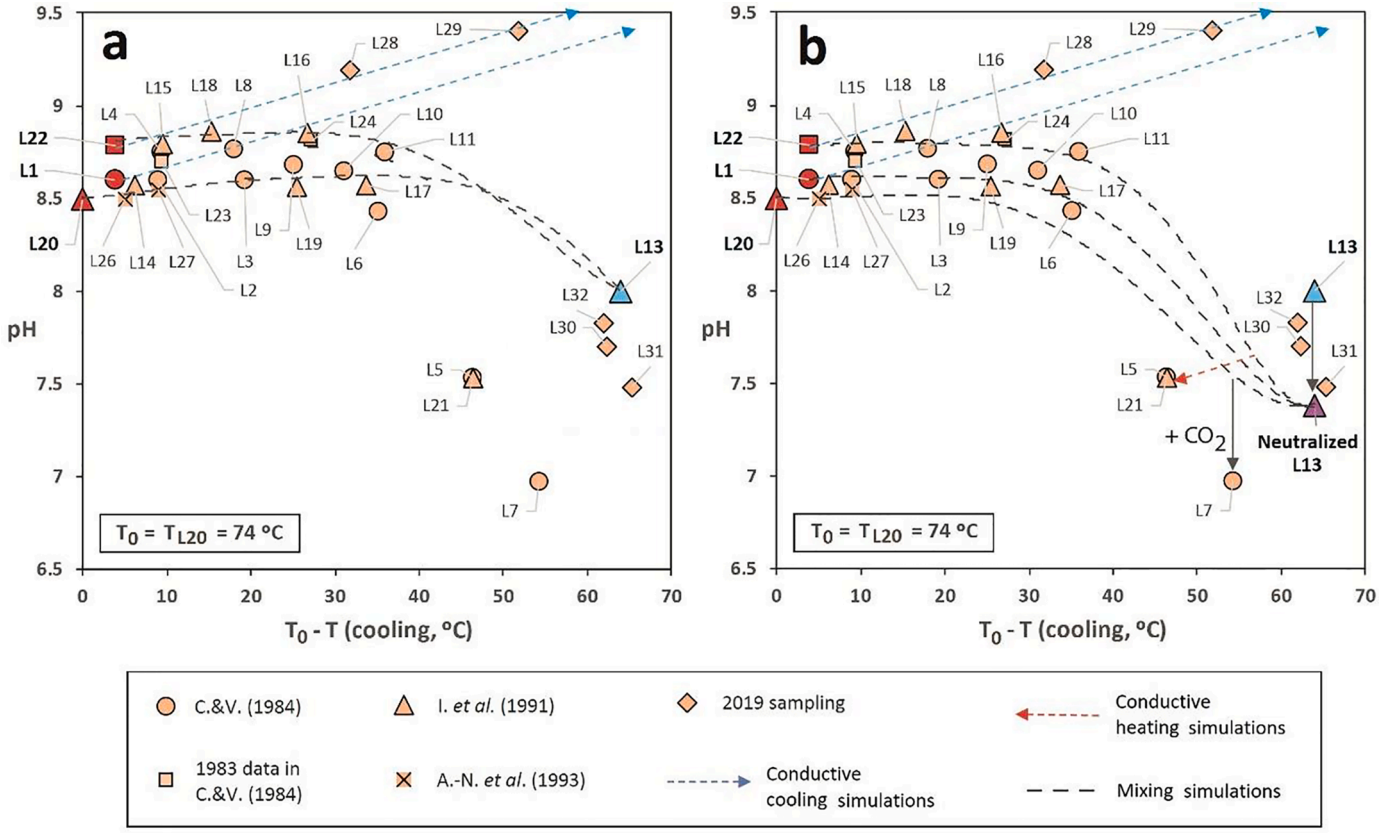

Fig. 6. Comparison between the simulation results and the natural system data (analytical data). Several mixing simulation paths are shown: between the thermal end members (L1, L20 and L22) and two cold end members, the sample L13 (6a) and a theoretical solution (6b) obtained by neutralising the anomalous pH of L13 to the expected value according to the logarithmic trend shown in Fig. 2.d. The cooling simulation and heating paths are shown for different thermal end members and mixing ratios, although different combinations of mixing and conductive cooling or heating can be interpreted for certain springs.

a CO_2 ingas process (up to a log pCO2 = -3.29) over a water originally similar to L22.

4.4. Main features, lessons learnt and some practical implications of the hydrogeochemical model

Throughout the results shown in the previous sections, the hydrogeochemical model of the processes and the evolution of the hydrochemical parameters of groundwater has been established, as summarised in the conceptual scheme shown in Fig. 7. This conceptual model includes the main processes and characteristics of the system, from the descent of the water towards the deep reservoir and the equilibrium with the granitic materials to the secondary processes of mixing, conductive cooling and CO_2 transfer that take place during the ascent of the hydrothermal solutions to the springs.

Regarding the geothermometrical results, it can be stated that the only way to get a good convergence in the saturation index variation with temperature is under open system conditions, imposing a re-equilibrium with kaolinite and calcite. This means that the effects of mass transfer on the saturation indices during the water ascent are not negligible in this system, although they have very little effect on pH variation, which is mainly due to conductive cooling. Under these conditions, the simulation results give a range of temperatures in the reservoir for the two thermal end members of 118 ± 7°C for L1 and 113 ± 4°C for L22, in good agreement with the temperatures provided by the considered reliable geothermometers applied to L1, L20 and L22 (100 – 133 °C), once deduced that quartz is the silica phase in equilibrium at depth and after rejected the temperature obtained with β=1/3 by the Na-K-Ca geothermometer. The reservoir temperatures obtained for the samples with the highest spring temperature (L1, L20 and L22) are similar but higher in L1 and L22 which, together with a more precise equilibrium convergence of quartz, albite and potassium feldespar, indicate that L1 and L22 are probably the most representative thermal end members. Thus, in summary, although the temperatures obtained with all the geothermometers, calibrations and samples range from 89°C to 133°C, if the temperatures obtained with samples L1 and L22 are considered more representative, and the equilibrium with chalcedony is rejected, a more precise range of 108 - 133°C for geothermometers can be finally proposed, in good agreement with the range of 117 ± 8°C obtained by the geothermometrical simulations (gathering the two T ranges obtained for L1 and L22).

It is also important to note that the waters in the deep reservoir have

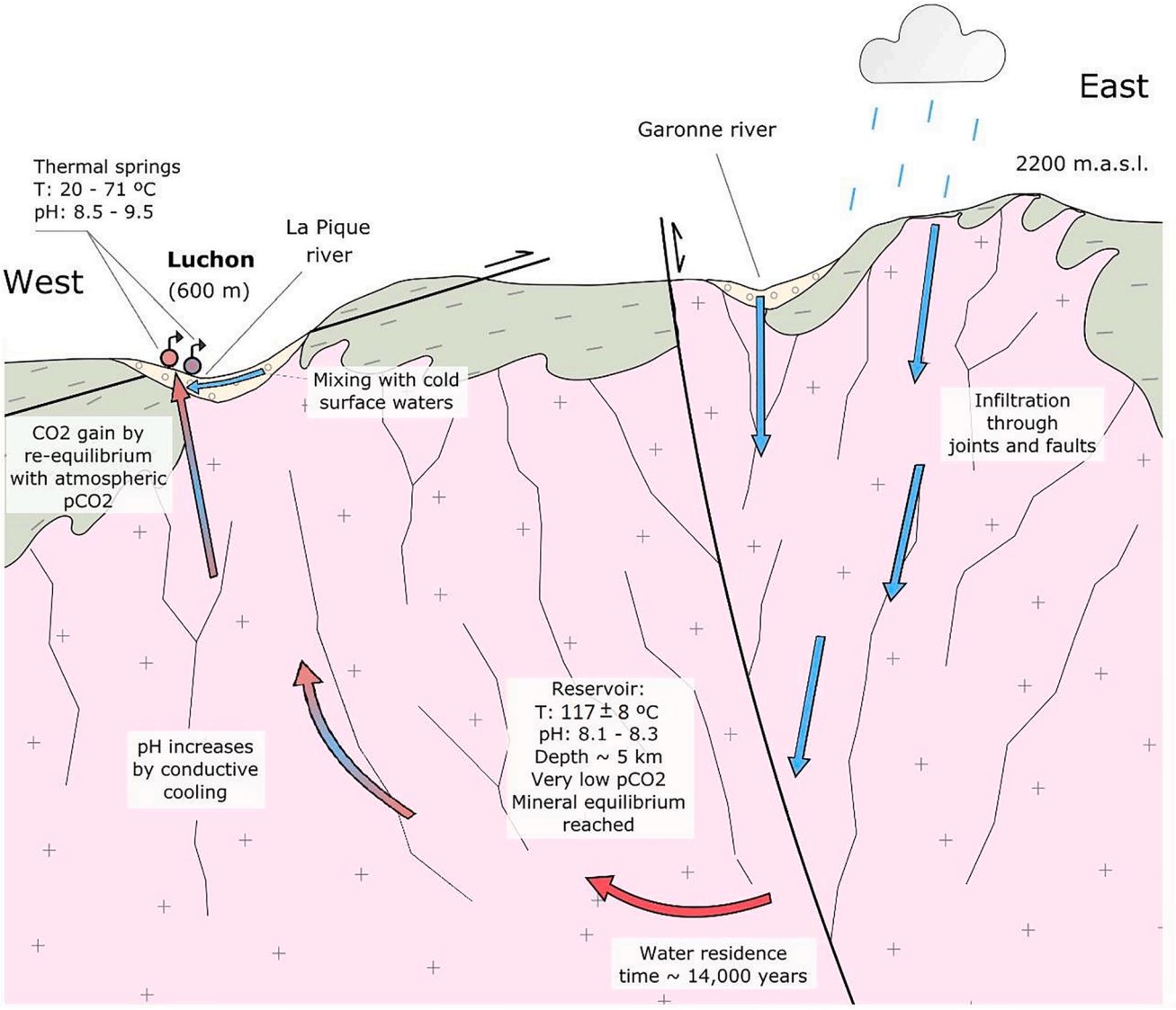

Fig. 7. Conceptual model (not to scale) of the main hydrogeochemical features of the Luchon hydrothermal system and its evolution, according to the hydrogeochemical model developed in this work. The water residence time has been obtained from Lopoukhine and Vigouroux (1998).

very low CO_2 partial pressures which, at large, also characterise the alkaline water systems in granite materials. These low CO_2 pressures, in the range of $10^{-4.59}$ – $10^{-2.59}$ atm can be explained in terms of some chemical reactions likely to take place at depth. Since these waters are in contact with granites, it is expected that the main reactions during the water-rock interaction constitute the alteration of aluminosilicates. The dissolution of these minerals consumes large amounts of CO_2 so that, for instance, in the dissolution of albite and anorthite 2 moles of CO_2 are consumed for each mole of Ca and Na, respectively, as shown in reactions 1 and 2.

$$2NaAlSi_3O_8 + 11H_2O + 2CO_2 \rightarrow 2Na^+ + Al_2Si_2O_5(OH)_4 + 4H_4SiO_4 + 2HCO_3^- \quad (2)$$

$$CaAl_2Si_2O_8 + 3H_2O + 2CO_2 \rightarrow Ca^{2+} + Al_2Si_2O_2(OH)_2 + 2HCO_3^- \quad (3)$$

In turn, these reactions, with or without the contribution of calcite dissolution, can induce calcite precipitation (see reaction 3) during the descent of the water to the deep reservoir, which would also be favoured by the temperature increase and the retrograde calcite solubility.

$$Ca^{2+} + 2HCO_3^- \rightarrow CaCO_3 + CO_2 + H_2O \quad (4)$$

These processes would result in a progressive decrease in the CO_2 partial pressures, which is consistent with the low CO_2 pressures calculated in PHREEQC for the deep reservoir, and the same processes also would explain the calcite equilibrium deduced at depth. This implies that the calcite precipitation could take place as a CO_2 mineral trapping mechanism in the context of a geological storage of CO_2 in granitic materials hosting groundwaters with similar physicochemical parameters. Furthermore, after the injection of the CO_2, the dissolution of the granite aluminosilicates is expected to be strongly increased, so this could also induce higher amounts of subsequent calcite precipitation and CO_2 trapping. These processes will be studied in future works on this and other alkaline hydrothermal systems hosted in granitic rocks.

The pH values obtained from the geothermometrical modelling for the waters in the deep reservoir (approximately 8.1 - 8.3) can be explained by the CO_2 consumption implicit in the reactions above. However, these values are significantly lower than the ones measured in many springs (up to 9.48) that are actually characterised as “alkaline thermal” waters due to this feature. This difference in the values between depth and surface indicates that the high pH values are increased by the conductive cooling during the ascent of the waters. This conclusion is consistent, and has been quantified, with the conductive cooling simulations, that show a linear increase of 0.0135 pH units per degree°C of cooling. This rate of increase is in good agreement with some previous observations in similar systems (e.g. Auqué *et al.,* 1998; Asta *et al.*, 2010 and references therein), as well as with the results obtained in controlled cooling experiments performed with alkaline thermal solutions (Michard and Fouillac, 1980). The magnitude of this pH increase by conductive cooling should be considered in other granite-hosted alkaline geothermal systems, for example, in the exploration and selection of sites for Deep Geological Repositories, or in geothermal exploration, since the alkaline character of the waters sampled in thermal springs or even in shallow boreholes may be much higher than that in the deep reservoir waters.

The mixing simulations have enabled to quantify the previously inferred pH buffering capacity of alkaline solutions. The pH remains constant up to mixing proportions of approximately 50% with surface water, mainly due to the high activity of the acid-base pair of the silica system. The modelling results for this process highlight the importance of considering the pH buffering capacity with regard to certain practical implications, such as in the context of the Deep Geological Disposal of nuclear wastes in granitic materials. This importance is justified by the sensitivity of the properties of certain engineering barriers, such as the bentonite barrier, to possible changes in the pH of the groundwater with which they will be in contact (e.g. Ye *et al.*, 2014). In this same context, the mixing between alkaline groundwaters and surface waters is expected to take place under the future glaciation scenarios contemplated in the long-term safety assessments of Deep Geological Disposal concepts (e.g. Näslund *et al.*, 2013).

The comparison between the simulations and the natural system also suggests that the variability observed in the thermal end members is likely to be due to a control from the surface processes and not to a variability in the deep reservoir conditions, which are expected to be constant considering the long residence times and the mineral equilibrium reached at depth. A final important practical outcome from this quantification of the effect of surface waters in the system is the evidence that the thermal waters are highly susceptible to contamination with origin in these surface waters. Besides, the loss of alkalinity due to mixing in proportions higher than 50% of surface cold waters is another sign of the susceptibility of the thermal waters to the loss of their quality for their use in balneotherapy. This susceptibility has been indicated also by previous authors in similar systems of the Pyrenees (e.g. Asta *et al.*, 2017) and, according to the simulation results explained above, in this system this should also be considered when planning the analytical control, not only of thermal but also of the surface waters, as well as the activities that could contaminate surface waters in the surroundings of the spa resort.

6. Conclusions

Geochemical modelling and classical geochemical calculations have been used to characterise the Luchon alkaline hydrogeothermal system. The modelling results indicate that the hydrogeochemical variability of the system, visible in its numerous thermal springs, is mainly controlled by the following processes: (1) mixing between thermal and cold groundwaters; (2) conductive cooling superimposed on some of the thermal waters and 3) transfer of CO_2 in particular springs. Comparing the simulated reaction paths and the analytical data, the best fit obtained indicates that most of the springs result from different mixing ratios between a thermal end member aproximately represented by sample L1, which is affected by an edaphic or atmospheric CO_2 contamination (of about 168 μmol/L) at surface, and a cold end member represented by a theoretical solution (L13 with restored or neutralised pH to the theoretical trend) similar to the surface water sampled in La Pique river (L31), in the surroundings of the Luchon spa resort. This river collects the water from the shallow alluvial reservoir, where the mixing probably takes place.

Apart from mixing, several springs are also affected, to a different extent, by conductive cooling. The simulations also reveal that most alkaline thermal waters in this system are characterised by a high pH-buffering capacity during the mixing, so that the high pH values of the thermal end member are maintained even up to mixing proportions of 50% with cold waters. The speciation-solubility calculations carried out have enabled to establish that this pH-buffering capacity is provided by the active acid-base pairs $H_4SiO_4^0/H_3SiO_4^-$ and, to a lesser extent, HCO_3^-/CO_3^{2-}. Similar processes (pH-buffering or mixing of groundwaters) are expected to take place in the deep repositories for radioactive wastes disposal in granitic rocks and that is why these granite-hosted hydrothermal systems of alkaline waters, like the one studied in this work, constitute a good opportunity to contrast the applicable geochemical modeling techniques.

Regarding the conditions in the deep reservoir, the results obtained by the geothermometrical modeling provide reservoir temperatures of 117 ± 8 °C, consistent with the temperatures ranging from 108 to 133 C° predicted by the most reliable of the classical chemical geothermometers applied to the most representative samples of the thermal end-member, L1 and L22. This agreement supports the conclusion that the thermal solutions in the deep reservoir have reached equilibrium with quartz, albite, potassium feldspar, zoisite and prehnite, and that re-equilibirum processes with kaolinite and calcite take place during their ascent to the surface, although their effect on the pH is negligible

compared with the effects due to conductive cooling. It is important to highlight that considering only these re-equilibria through the open system simulation conditions an admissible accuracy of the simulation results has been reached. The deduced equilibrium with calcite at depth indicates that this mineral is probably precipitating during the descent of the water to the reservoir, which has an interesting implication as a possible CO_2 mineral trapping mechanism in granitic materials hosting alkaline groundwaters with similar physicochemical properties.

The geothermometrical simulations also indicate that the pH values in the reservoir (8.1 – 8.3) are lower than the values measured in the springs (up to 9.48) which reveals that the high pH values of the thermal waters in this system are not only inherited from the deep reservoir but strongly enhanced by conductive cooling as the waters rise to the surface. This is also consistent with the conductive cooling simulations, that show a linear increase of pH with a variation rate of 0.0135 pH units per degree °C of cooling.

Based on these results it can be said that the spatial and temporal variability observed in the thermal end member is controlled by the secondary processes mentioned, and it is not related to changes in the deep reservoir conditions. Furthermore, the influence on the thermal waters of their mixing with surface cold waters reveals the high susceptibility of this system to contamination processes from the surface waters, and, therefore, to a loss of their quality for their use in balneotherapy. Thus, considering the possible economical implications of this susceptibility, it is advisable to maintain a periodic analytical control, not only of the thermal waters, but also of the surface waters in Luchon near the spa resort.

Further investigations are needed, through the characterization of different alkaline hydrothermal systems hosted in granitic rocks, to better establish the applicability conditions of geochemical and geothermometrical modelling techniques. Indeed, the variability observed in this system regarding the hydrogeochemical processes and the parameters of the hydrothermal solutions suggest that the comparison with other systems of this type would be necessary to extensively determine the most reliable geothermometers, the phases suitable to reach equilibrium in the deep reservoir or the re-equilibriums during the ascent that must be considered to establish the appropriate simulation conditions. Moreover, further geochemical modelling work in these granitic systems could be useful to better understand how the hydrogeochemical parameters of the reservoir and the secondary processes such as mixing or cooling could control the expected chemical reactions of interest for the geological storage of CO_2 in granitic materials, such as those related with porosity changes or CO_2 mineral trapping.

CRediT authorship contribution statement

Jon Jiménez: Conceptualization, Methodology, Investigation, Software, Formal analysis, Validation, Data curation, Visualization, Resources, Writing – original draft, Writing – review & editing. **María J. Gimeno:** Supervision, Project administration, Funding acquisition, Validation, Resources, Writing – review & editing. **Luis F. Auqué:** Supervision, Project administration, Validation, Resources, Writing – review & editing.

Declaration of Competing Interest

The authors declare that they have no known competing financial interests or personal relationships that could have appeared to influence the work reported in this paper.

Data Availability

The research data are provided in the supplementary material.

Acknowledgements

The author Jon Jiménez has worked in this study thanks to a FPU scholarship from the Ministry of Education and Professional Training of Spain, for the training of university teachers (ref. FPU19/00870). This study is part of the research activities of the Geochemical Modelling Group (University of Zaragoza; Aragón Government) and it has also been supported by the Earth Sciences Department from the University of Zaragoza. We want to thank the director of the Luchon spa and the Mayor of Luchon for giving the permision for sampling the accesible springs inside the spa facilities. We also thank Enrique Oliver, from the Geochemistry Laboratory of the Earth Sciences Department of the Unviersity of Zaragoza, and the analytical services (SAI) at the University of Zaragoza, for their help with the chemical analyses.

Supplementary materials

Supplementary material associated with this article can be found, in the online version, at doi:10.1016/j.geothermics.2022.102573.

References

Alaux-Negrel, G., Beaucaire, C., Michard, G., Toulhoat, P., Ouzounian, G., 1993. Trace-metal behaviour in natural granitic waters. J. Contam. Hydrol. 13, 309–325.
Appelo, C.A.J., Parkhurst, D.L., Post, V.E.A., 2014. Equations for calculating hydrogeochemical reactions of minerals and gases such as CO2 at high pressures and temperatures. Geochim. Cosmochim. Acta 125, 49–67.
Arnòrsson, S., Gunnlaugsson, E., Svavarsson, H., 1983. The chemistry of geothermal waters in Iceland. III. Chemical geothermometry in geothermal investigations. Geochim. Cosmochim. Acta 47, 567–577.
Asta, M.P., Galve, J.P., Gómez, J., Gimeno, M.J., Auqué, L.F., Acero, P., Lapuente, P., 2017. Temporal variability of secondary processes in alkaline geothermal waters associated to granitic rocks: the Caldes de Boí geothermal system (Spain). Geologica Acta 15, 67–87.
Asta, M.P., Gimeno, M.J., Auqué, L.F., Gómez, J., Acero, P., Lapuente, P., 2010. Secondary processes determining the pH of alkaline waters in crystalline rock systems. Chem. Geol. 276, 41–52.
Asta, M.P., Gimeno, M.J., Auqué, L.F., Gómez, J., Acero, P., Lapuente, P., 2012. Hydrochemistry and geothermometrical modelling of low-temperature Panticosa geothermal system (Spain). J. Volcanol. Geotherm. Res. 235, 84–95.
Auqué, L.F., Mandado, J., Gimeno, M.J., López, P.L., Gómez, J., 1996a. Los sistemas geotermales del Pirineo Central. I. Caracteres geoquímicos y fisicoquímicos de los manantiales termales. Estudios Geológicos 52, 161–173.
Auqué, L.F., Mandado, J., López, P.L., Gimeno, M.J., 1996b. Los sistemas geotermales del Pirineo Central. II. Resultados de la aplicación de técnicas geotermométricas. Estudios Geológicos 53, 45–54.
Auqué, L.F., Mandado, J., López, P.L., Lapuente, M.P., Gimeno, M.J., 1998. Los sistemas geotermales del Pirineo Central. III. Evaluación de las condiciones en profundidad y evolución de las soluciones hidrotermales durante su ascenso. Estudios Geológicos 54, 25–37.
Ball, J.W., Nordstrom, D.K., 2001. User's manual for WATEQ4F with revised thermodynamic database and test cases for calculating speciation of major, trace and redox elements in natural waters. U.S. Geological Survey. Water-Resources Investigations Rep. 91–183.
Bethke, C.M., 1996. Geochemical Reaction Modeling. Oxford University Press, p. 397.
Bosch, B., Risler, J., Soule, J., Ternet, Y., 1981. Etude hydrogéologique des sources minérales des thermes de Luchon. Rapport du BRGM (Bureau de Recherches Géologiques et Minières 81.
Buil, B., Gómez, P., Turrero, M.J., Garralón, A., Lago, M., Arranz, E., De la Cruz, B., 2006. Factors that control the geochemical evolution of hydrothermal systems of alkaline water in granites in Central Pyrenees (Spain). J. Iberian Geol. 32 (2), 283–302.
Chevalier-Lemire, G., Pigassou, R., Rigaill, R., Vilmus, T., 1990. Etude des variations naturelles du debit des sources thermales à Luchon (Haute-Garonne, France) par modèle hydrologique global pluies-débits. Hydrogéologie (4), 287–296.
Choi, B.Y., Yun, S.T., Kim, K.H., Choi, H.S., Chae, G.T., Lee, P.K., 2014. Geochemical modeling of CO2–water–rock interactions for two different hydrochemical types of CO2-rich springs in Kangwon District. Korea. Journal of Geochemical Exploration 144, 49–62.
Clariana, P., García-Sansegundo, J., Gavaldá, J., 2009. The structure in the Bagneres de Luchon and Andorra cross sections (Axial Zone of the central Pyrenees). Trabajos de geología 29, 175–181.
Criaud, A., Vuataz, D., 1984. Etude géochimique et géothermique des eaux sulfurées sodiques de Luchon, Pyrénées. Rapport du BRGM (Bureau de Recherches Géologiques et Minières) 84. URL infoterre.brgm.fr/rapports/84-SGN-384-IRG.pdf (accessed 04.30.2022.
Fouillac, C., Michard, G., 1981. Sodium/lithium ratio in water applied to geothermometry of geothermal reservoirs. Geothermics 10, 55–70.
Fournier, R.O., 1977. Chemical geothermometers and mixing models for geothermal systems. Geothermics 5, 41–50.

Fournier, R.O., Potter II, R.W., 1982. An equation correlating the solubility of quartz in water from 25 to 900 C at pressures up to 10,000 bars. Geochim. Cosmochim. Acta 46 (10), 1969–1973.
Fournier, R.O., Truesdell, A.H., 1973. An empirical Na–K–Ca geothermometer for natural waters. Geochim. Cosmochim. Acta 37, 1255–1275.
García-Sansegundo, J., Ramírez Merino, J.I., Rodríguez Santisteban, R., Leyva, F., 2013. Mapa Geológico de España 1:50.000, Hoja n° 148 (Vielha) y Memoria. IGME, Madrid, p. 66.
Giggenbach, W.F., Gonfiantini, R., Jangi, B.L., Truesdell, A.H., 1983. Isotopic and chemical composition of Parbati valley geothermal discharges. N.W. Himalaya. India. Geothermics 12, 199–222.
Hangx, S.J., Spiers, C.J., 2009. Reaction of plagioclase feldspars with CO2 under hydrothermal conditions. Chem. Geol. 265 (1–2), 88–98.
Iundt, F., Pigassou, R., Rigaill, R., 1991. L'évolution des sulfures depuis l'émergence jusqu'à la distribution. Exemple de Bagnères-de-Luchon. J. français d'hydrologie 22, 17–27.
Kaieda, H., Ueda, A., Kubota, K., Wakahama, H., Mito, S., Sugiyama, K., Ozawa, A., Kuroda, Y., Sato, H., Yajima, T., Kato, K., Ito, H., Ohsumi, T., Kaji, Y., Tokumaru, T., 2009. Field experiments for studying on CO2 sequestration in solid minerals at the Ogachi HDR geothermal site, Japan. In: Proceedings of the 34th workshop on geothermal reservoir engineering. Stanford University.
Liu, L., Suto, Y., Bignall, G., Yamasaki, N., Hashida, T., 2003. CO2 injection to granite and sandstone in experimental rock/hot water systems. Energy Convers. Manage. 44 (9), 1399–1410.
Lopoukhine, M., Vigouroux, P., 1998. Memento technique des Eaux Minérales. Rapport du BRGM 40145. R.
Michard, G., 1983. Recueil de donnees thermodynamiques concernant les equilibres eaux-mineraux dans les reservoirs geothermaux. Rapp. Comm. Eur. Brussels EUR8590 FR.
Michard, G., 1990. Behaviour of major elements and some trace elements (Li, Rb, Cs, Sr, Fe, Mn, W y F) in deep hot waters from granitic areas. Chem. Geol. 89, 117–134.
Michard, G., Roekens, E., 1983. Modelling of the chemical composition of alkaline hot waters. Geothermics 12, 161–169.
Michard, G., Sanjuan, B., Criaud, A., Fouillac, e, Pentcheva, E.N., Petrov, P.S., Alexieva, R., 1986. Equilibria and geothermometry in hot waters from granites of S. W. Bulgaria. Geochem. J. 20, 159–171.
Michard, G., Fouillac, C., 1980. Controle de la composition chimique des eaux thermales sulfurées sodiques du Sud de la France. Géochimique Des Interactions Entre Les eaux, Les Mineréux Et Les Roches (Y. Tardy. Elements, Tarbes, pp. 147–166.
Michard, G., Grimaud, D., D'Amore, F., Fancelli, R., 1989. Influence of mobile ion concentrations on the chemical composition of geothermal waters in granitic areas. Example of hot springs from Piemonte (Italy). Geothermics 18 (5–6), 729–741.
Näslund, J.O., Brandefelt, J., Liljedahl, L.C., 2013. Climate considerations in long-term safety assessments for nuclear waste repositories. Ambio 42, 393–401. https://doi.org/10.1007/s13280-013-0406-6.
Parkhurst, DL, Appelo, CAJ (2013). Description of Input and Examples for PHREEQC Version 3. A Computer Program for Speciation, Batch Reaction, One Dimensional Transport, and Inverse Geochemical Calculations. In: *Techniques and Methods* (U.S. Geological Survey, Ed.), Book 6, Chap. A43. U.S.
Porowski, A., Dowgiałło, J., 2009. Application of selected geothermometers to exploration of low-enthalpy thermal water: the sudetic geothermal region in Poland. Environ. Geol. 58, 1629–1638.
Ré, C.L., Kaszuba, J.P., Moore, J.N., McPherson, B.J., 2014. Fluid–rock interactions in CO2-saturated, granite-hosted geothermal systems: implications for natural and engineered systems from geochemical experiments and models. Geochim. Cosmochim. Acta 141, 160–178.
Reed, M.K., Spycher, N., 1984. Calculation of pH and mineral equilibria in hydrothermal waters with application to geothermometry and studies of boiling and dilution. Geochim. Cosmochim. Acta 48, 1479–1492.
Suto, Y., Liu, L., Yamasaki, N., Hashida, T., 2007. Initial behavior of granite in response to injection of CO2-saturated fluid. Appl. Geochem. 22 (1), 202–218.
Truesdell, A.H., 1976. Geochemical techniques in exploration. Summary of section III. In: Proceedings of the Second United Nations Symposium on the Development Y Use of Geothermal Resources. San Francisco (California), pp. 3–29.
Vandelanoote, R., 1984. Trace Element Geochemistry in Thermal Waters (E. Pyrenees). Thesis, University of Anvers, p. 489.
Vera, J.A., 2004. Geología De España. Sociedad Geológica De España. Madrid, p. 884.
Wakahama, H., Mitoa, S., Ohsumi, T., Ueda, A., Yajima, T., Satoh, H., Sugiyama, K., Ozawa, A., Ajima, S., Todaka, N., Sato, T., Kato, M., Kaji, Y., Tokumarui, T., Kaieda, H., Kubota, K., 2009. A Concept of CO2 Georeactor sequestration At the Ogachi HDR Site, 1. NE Japan. Energy Procedia, pp. 3683–3689.
White, A.F., Bullen, T.D., Vivit, D.V., Schulz, M.S., Clow, D.W., 1999. The role of disseminated calcite in the chemical weathering of granitoid rocks. Geochim. Cosmochim. Acta 63 (13–14), 1939–1953.
White, A.F., Schulz, M.S., Lowenstern, J.B., Vivit, D.V., Bullen, T.D., 2005. The ubiquitous nature of accessory calcite in granitoid rocks: implications for weathering, solute evolution, and petrogenesis. Geochim. Cosmochim. Acta 69 (6), 1455–1471.
Ye, W.M., Zheng, Z.J., Chen, B., Chen, Y.G., Cui, Y.J., Wang, J., 2014. Effects of pH and temperature on the swelling pressure and hydraulic conductivity of compacted GMZ01 bentonite. Appl. Clay Sci. 101, 192–198.
Zhu, C., Anderson, G., Burden, D.S., 2002. Environmental Applications of Geochemical Modeling. Cambridge University Press.
Zwart, H.J., y De Sitter, L.U., 1979. The geology of the Central Pyrenees. Leidse Geologische Mededelingen 50, 1–74.